Quaternary International xxx (xxxx) xxx–xxx

Contents lists available at ScienceDirect

Quaternary International

journal homepage: www.elsevier.com/locate/quaint

Geomorphological changes in the coastal area of Farasan Al-Kabir Island (Saudi Arabia) since mid Holocene based on a multi-proxy approach

Kosmas Pavlopoulos[a,*], Olga Koukousioura[b], Maria Triantaphyllou[c], Dimitris Vandarakis[d,f], Solène Marion de Procé[e], Vassilia Chondraki[d], Eric Fouache[a], Vasilios Kapsimalis[f]

[a] Paris Sorbonne University Abu Dhabi, Geography and Planning Department, P.O. 38044, Abu Dhabi, United Arab Emirates
[b] Aristotle University of Thessaloniki, School of Geology, 54124, Thessaloniki, Greece
[c] National and Kapodistrian University of Athens, Faculty of Geology and Geoenvironment, 15784, Athens, Greece
[d] Harokopio University, Geography Department, 70 El. Venizelou St, 15671, Athens, Greece
[e] Université Paris 1 – Panthéon Sorbonne, Archéologies et Sciences de l'Antiquité, (équipe APOHR, UMR 7041), Nanterre, France
[f] Hellenic Centre for Marine Research, Institute of Oceanography, 46.7 km Athens-Sounio Ave, 19013, Anavyssos, Greece

ARTICLE INFO

Keywords:
Reefal sedimentation
Benthic foraminifera
Bulk mineralogy
Geochemistry
Farasan
Wadi matar
Red sea

ABSTRACT

The geomorphological evolution of the southeastern coastal area of Farasan Al-Kabir Island (Saudi Arabia) is revealed by the mapping of modern landforms and a multi-proxy and high spatial resolution study including grain size, particulate organic carbon, mineralogy, element geochemistry, benthic foraminifera analysis and radiocarbon dating of a 3.3-m long sediment core. The modern geomorphological features comprise a variety of arid landforms, such as plateau, cliffs and pediments of Pleistocene coral limestones, playa depressions located on plateau surfaces, alluvial fans, butte and sandy beaches. The mid Holocene evolution of the borehole area is resulted from the detailed analysis of five sedimentary units detected along the core Matar-1, and includes three distinct stages: (a) from 5253 ± 223 y cal BP to 3138 ± 223 y cal BP, carbonate coarse-grained material consisting of coral fragments, molluscs, calcareous algae and benthic foraminifera are deposited on a shallow marine fringing reefal platform, which becomes progressively a nearshore backreef (around 3675 ± 215 y cal BP), and later (around 3138 ± 223 y cal BP) a reef ramp; (b) since 3040 ± 220 y cal BP the borehole area obtains the characteristics of a high-energy beach that receives increasing inputs of terrigenous material; (c) subsequently, a supratidal backshore setting is established influenced mostly by terrestrial processes and occasionally by marine processes, as it is indicated by the decreasing and sometimes sporadic presence of benthic foraminifera, and recently, a sedimentary veneer consisting of terrigenous, carbonate and evaporite material is formed by terrestrial, mainly wadi and aeolian, processes.

1. Introduction

Holocene environmental changes of coastal areas with a high temporal resolution, i.e. from centennial to millennial time scale, can be derived by the multi-proxy analysis of sediment cores (Morhange et al., 2000; Bos et al., 2005; Triantaphyllou et al., 2003, 2010; Di Rita et al., 2011). Variations in granulometric, mineralogical and geochemical composition along the cores provide indications for the origin and fate of deposits, the sedimentary dynamics, and diagenetic processes during the post-depositional time interval (Dellwig et al., 2000; da Conceição Freitas et al., 2003; Dinelli et al., 2012; Sallun et al., 2012). Furthermore, the study of benthic foraminifera assemblages together with radiocarbon dating can reveal the succession of past environmental conditions and, therefore, the alteration of physiographical settings (Cann et al., 1988, 2000; Cearreta et al., 2003; Horton et al., 2007; Xiang et al., 2008; Koukousioura et al., 2012).

The long term geomorphological evolution of a location, which nowadays is a coast, is mainly resulted from the interplay between the relative sea level (RSL) change and the sedimentation pattern (Thom and Roy, 1985; Pirazzoli and Pluet, 1991; Semeniuk, 1995; Dias et al., 2000). RSL change is the resultant of eustatic changes, glacio-hydro-isostatic variations, and regional vertical displacement trends, which are a function of tectonism (i.e., structural deformation of the crust, co-seismic earthquake movements, aseismic vertical creep, fault displacements, large-scale tectonic crustal movements associated with plate boundaries and plate movements), sediment budget, sediment load isostasy, and sediment compaction (also due to anthropogenic activities) (Lambeck and Chappell, 2001; Lambeck et al., 2011). In addition

* Corresponding author.
E-mail address: kosmas.pavlopoulos@psuad.ac.ae (K. Pavlopoulos).

https://doi.org/10.1016/j.quaint.2018.06.004
Received 29 August 2017; Received in revised form 5 April 2018; Accepted 2 June 2018

to RSL fluctuations, depositional and erosive processes can alter the physiographic characteristics of shallow marine areas or coastal lowlands, infilling and deepening the surface morphology, respectively (Swift, 1968; Kraft, 1971; Roy et al., 1980). The type of sedimentation prevailing in a region depends of a variety of climatic, oceanographic and biological parameters, such as the air and water temperature, precipitation and evaporation, wind regime, tidal range, water transparency, primary productivity, salinity and water circulation pattern (Reading, 1996).

In arid environments, where terrigenous sediment delivery is limited, coasts are dominated by biogenic sand comprising carbonate skeletons of corals and other reef organisms (Fryberger and Goudie, 1981; Montaggioni, 2005). The sand can be derived by the erosion of both adjacent shallow-water seabed and the bolson (arid drainage basin) transported through local seawater currents, terrestrial runoff, wadis (ephemeral streams) and wind (Friedman, 1968; Purser and Seibold, 1973; Fabricius, 2005).

The formation of coral reef systems in the Red Sea has initiated by the Pliocene (2.6–5.3 Ma) (Klaus, 2015). During the Pleistocene (2.6–0.01 Ma) reefs continued to be built as carbonate platforms, which were shaped over time by tectonics, irregular uplift of the underlying Miocene evaporites, and periods of interruption or dissolution of carbonate sedimentation during eustatic sea level fluctuations (Bosence, 2005; Klaus, 2015; Rowlands and Purkis, 2015). Recent reefs have been proliferated on the Quaternary substrate just after the Holocene sea level highstand (Behairy, 1983; Heiss, 1994). The coral reef coastal geomorphology includes: (a) a shallow platform, which at its seaward end a continuous marginal reef occurs; (b) a rocky intertidal zone with erosional features (notches and cliffs) or a beach consisting of gravel and sand with abundant shell material swept up from the sea; and (c) sand dunes at the backshore zone or an alluvial fan created by wadis (Mansour and Madkour, 2015). The above coastal landscape supports flora and fauna of high diversity and abundance (Bruckner et al., 2012; Berumen et al., 2013), and therefore, it was a hospitable habitat for the early human (Bailey et al., 2007, 2015). The first evidence of Quaternary occupation dates back to at least 150,000 years and perhaps could extend to 1 million years or more (Bailey, 2009, 2015).

The purpose of this study is: (a) to describe the recent geomorphological features of the southern part of Farasan Al-Kabir Island (Saudi Arabia); and (b) to reconstruct the coastal paleoenvironments since the mid Holocene based on the analysis of a 3.3-m long sediment core. A multidisciplinary approach was selected to reveal short-term changes, combining lithological, element geochemical, micropalaeontological (benthic foraminifers), bulk mineralogical, and isotopic dating (^{14}C) analyses.

2. The study area

2.1. Physiographic and geological setting

The Farasan Bank lies in the southeastern part of the Red Sea, offshore the southwest Saudi Arabian coast (Fig. 1). The Bank consists of more than 128 islands and covers a total land area of approximately 600 km^2 (Khalil, 2012). The two main islands of the Farasan insular are Al Kabir and Sajid. Both islands are elongated and orientated alongside to the rift/ridge axis of the Red Sea. Farasan Al Kabir is the largest island of the archipelago having a length of 60 km, width of 5–8 km and a surface area of 381 km^2. The relief is low, with an average and maximum elevation of ~15 m and 75 m above mean sea level, respectively. They comprise coral reef platforms, which have been uplifted and deformed by salt tectonics (Dabbagh et al., 1984; Almalki et al., 2015).

The Farasan Bank is underlain by Tertiary and Quaternary formations deposited within the Red Sea basin (Macfadyen, 1930; Khalil, 2012). The lithology and structure of these rocks reflect changes in the tectonic regime of the area, produced in response to the rifting of the Arabian Nubian Shield along the Red Sea axis (Bantan, 1999; Almalki et al., 2015). The main geological units observed in Farasan Islands are (Almalki and Bantan, 2016): (a) Quaternary surficial deposits consisting mainly of white biogenic beach sand enriched in remains of corals, molluscs, calcareous algae and benthic foraminifera (Abu-Zied et al., 2011; Bantan and Abu-Zied, 2014); (b) Pleistocene coral limestones outcropping on many areas in Farasan Al-Kabir and Sajid Islands. This unit comprises reef facies, intercalated with beds very rich in pelecypod and gastropod shells, bryozoan, foraminifera, coralline algae and in-situ coral reefs; (c) Pliocene marly limestone with intersected isolated fossil-rich layers; (d) Miocene shale; and (e) Late-Middle Miocene evaporates. The total thickness of this unit is unknown because none of the research wells, collected from the broader area, penetrated its base.

The circular and linear (ridges) lineaments occurring on the surface morphology of Farasan Islands are probably formed by active salt diapirism (Bantan, 1999; Almalki et al., 2015).

2.2. Climate and tides

The Farasan Islands are affected by an arid and subtropical climate, with high mean annual temperatures (29.8 °C) and low rainfall (< 130 mm y^{-1}). However, humidity is high throughout the year, with the mean relative humidity in winter to range from 70% to 80% and in summer between 65% and 78% (El-Demerdash, 1996). There are two distinct monsoon seasons controlling the weather of the Farasan Bank area: the winter northeast monsoon from October to April and the summer southwest monsoon from May to September. Surface currents in the area are driven partly by winds and partly by density driven flows (to the southeast in summer and towards northwest during winter), which are established by heating and evaporation. Both orientations are parallel to the coast and to the elongation of the Farasan Islands (Bantan, 1999).

The main oceanographic feature of the Red Sea surrounding the Farasan Islands is the high salinity values of up to 35–40 psμ (Bemert and Ormond, 1981), as a consequence of the warm climate and the absence of any river fresh water influx. The sea surface temperature ranges approximately from 25 °C to 31 °C following a seasonal pattern, falls to about 21.5 °C at the thermocline (approx. 700 m), where it remains remarkably constant. The normal tides are small, with a peak of about 0.5 m. The shore in the study area is comprised predominantly of coral fringe reefs, lagoons and long sandy beaches. In winter, warmer and fresher water flows into the Red Sea near the surface, while cooler and saltier water flows into the Gulf of Aden at depth. During the summer the surface flow is reversed, and intermediate water from the Gulf of Aden flows into the Red Sea between the two outflowing layers (Siddall et al., 2002). Freshwater is provided mostly from underground water sites on the main islands supporting a remarkable faunal and floral diversity (Alwelaie et al., 1993; Hall et al., 2010; Al Mutairi et al., 2012; Alfarhan et al., 2016).

2.3. Human presence and archaeological context

The available marine and terrestrial recourses together with sheltered shores of Farasan Islands have been a key attraction for past settlers and seafarers (Bailey et al., 2007; Delagnes et al., 2013; Cooper and Zazzaro, 2014; Hausmann and Meredith-Williams, 2016). The Comprehensive Archaeological Survey Program carried out from the late 70's to early 80's brought into light numerous archaeological sites on the islands from the prehistory to the modern era (Zarins et al., 1981). Recent surveys in the southeastern tip of Farasan Al-Karib discover evidence of early occupation during the Ancient South Arabian period, i.e. the first half of 1st millennium BC, dated from buildings, pottery and inscriptions (Alsharekh and Bailey, 2014). A second phase of occupation is detected around the 1st-2nd centuries BC evidenced by the reoccupation of the early sites. It is noted that the oldest Roman military presence, two Latin inscriptions, has been documented by

Fig. 1. Location Map of the study area.

reused architectural elements in a modern village close to the Wadi Matar plain (Marion de Procé and Phillips, 2010). Finally, the third phase indicated by large scatters of late-antique ceramic wares (Cooper and Zazzaro, 2014). Although these settlements are located now about 3 km away from the shoreline, they provide an excellent field to study human activities in the southern Red Sea, especially in the context of the Roman long-distance trade (Fig. 3 a,b).

Nowadays, the population of the Farasan Islands is about 20 000 (census of 2010) inhabiting only the three main islands, i.e. Farasan Al-Kabir, Sajid and Qummah. The main human activity is fishing (Gladstone, 2002), while rain-fed agriculture and livestock grazing by camels, cattle, sheep and goats is very limited.

3. Methodology

The geomorphological processes and landscape evolution since Middle-Late Holocene were revealed by a multi proxy approach including geomorphological mapping, sediment sampling (coring), grain size, bulk mineralogical, element geochemical and micro-fauna analysis, and radiocarbon dating.

The geomorphological mapping conducted in the scale of 1:10 000 was based on the digital elevation models of Shuttle Radar Topography Mission (SRTM) and ASTER GDEM2, and the hardcopy topographic maps (scale 1:200.000) published in 1977 by the Soviet Military Topographic Mapping Service. The geological data were obtained from previous studies carried out in the Farasan Islands and Red Sea (Bantan, 1999; Khalil, 2012; Almalki et al., 2015; Almalki and Bantan, 2016). Furthermore, based on the altitude, slope and lithology, an automated geomorphometric analysis (Hammond, 1954; van Asselen and Seijmonsbergen, 2006; Piloyan and Konečný, 2017) was applied revealing a variety of arid landscapes, such as a reefal limestone plateau, escarpments or cliffs at the edge of the carbonate tableland, wadi riverbed, alluvial/colluvial fans and beach sands. The above results were verified, corrected or completed with new data obtained during a fieldwork mission in December 2014.

During the same geomorphological survey, a 3.30-m long sediment core (Core Matar-1) was collected by a manually drilling equipment (Fig. 3g and h). The geographic coordinates and the absolute altitude of the sampling site were acquired by a differential GPS. Core Matar-1 samples were collected, codified and stored for further laboratory analysis. Thirty nine (39) samples were split into sand and mud fractions by wet sieving through a 63 μm mesh. The coarse-grained subsamples were fractioned by dry sieving, whilst the finer granulometric fractions were determined by a particle size analyzer (Sedigraph III Plus, Micrometrics). Textural characterization and mean grain size of the samples were based on the Folk's nomenclature (Folk, 1974).

The Total Carbon (TC) was measured by a CHN elemental analyzer (EA-1108, Fisons Instruments) with the precision of the method being within 5% (Karageorgis et al., 2005), whilst the Particulate Organic Carbon (POC) portion was determined following the procedure described by Verardo et al. (1990) with the detection limit of the method being 2.3 μg g^{-1}. Carbonate content was estimated in weight percentage of the bulk sample (wt%) by the equation (TC - POC) x 8.33.

Mineralogical composition was determined by X-ray diffraction (XRD) of powdered six (6) non-oriented (bulk analysis) samples in a Rigaku D-Max/B system, employing Ni-filtered CuKa radiation and graphite monochromator. Randomly oriented samples were scanned over the interval 2-50° 2θ with a scanning speed of 1°/min, voltage of 40 kV and current of 20 mA.

The elemental geochemistry of twenty (20) sediment samples (< 2 mm) was determined using a Philips PW-2400 X-Ray Fluorescence (XRF) system, with the relative uncertainties of the system being within 2% for the major element concentrations (Al, Ca, Fe, K, Mg, Na, P, S, Si, Ti) and within 5% for the trace element concentrations (As, Ba, Bi, Br, Ce, Co, Cr, Cu, Hf, I, La, Mn, Mo, Nd, Ni, Pb, Rb, Sb, Sc, Sn, Sr, Th, V, Y, Zn, Zr) (Karageorgis et al., 2005). The vertical variation of elements or ratios of elements along a sediment core provides information about material pathways to and within marine environment. Rothwell and Croudace (2015) point out that Al, Fe, K, Si and Ti are abundant in terrigenous aluminosilicates and oxides; therefore, increased concentration of these elements in marine sediments implies aeolian, fluvial and/or runoff input. Moreover, the enhanced detrital load can be determined by the high ratio of Fe/Ca and Rb/Sr. Ca and Sr are related to biogenic carbonate production, while the ratios of Ba/Al and Br/Ti are proxies for export productivity.

Thirty nine (39) samples were used for micropaleontological

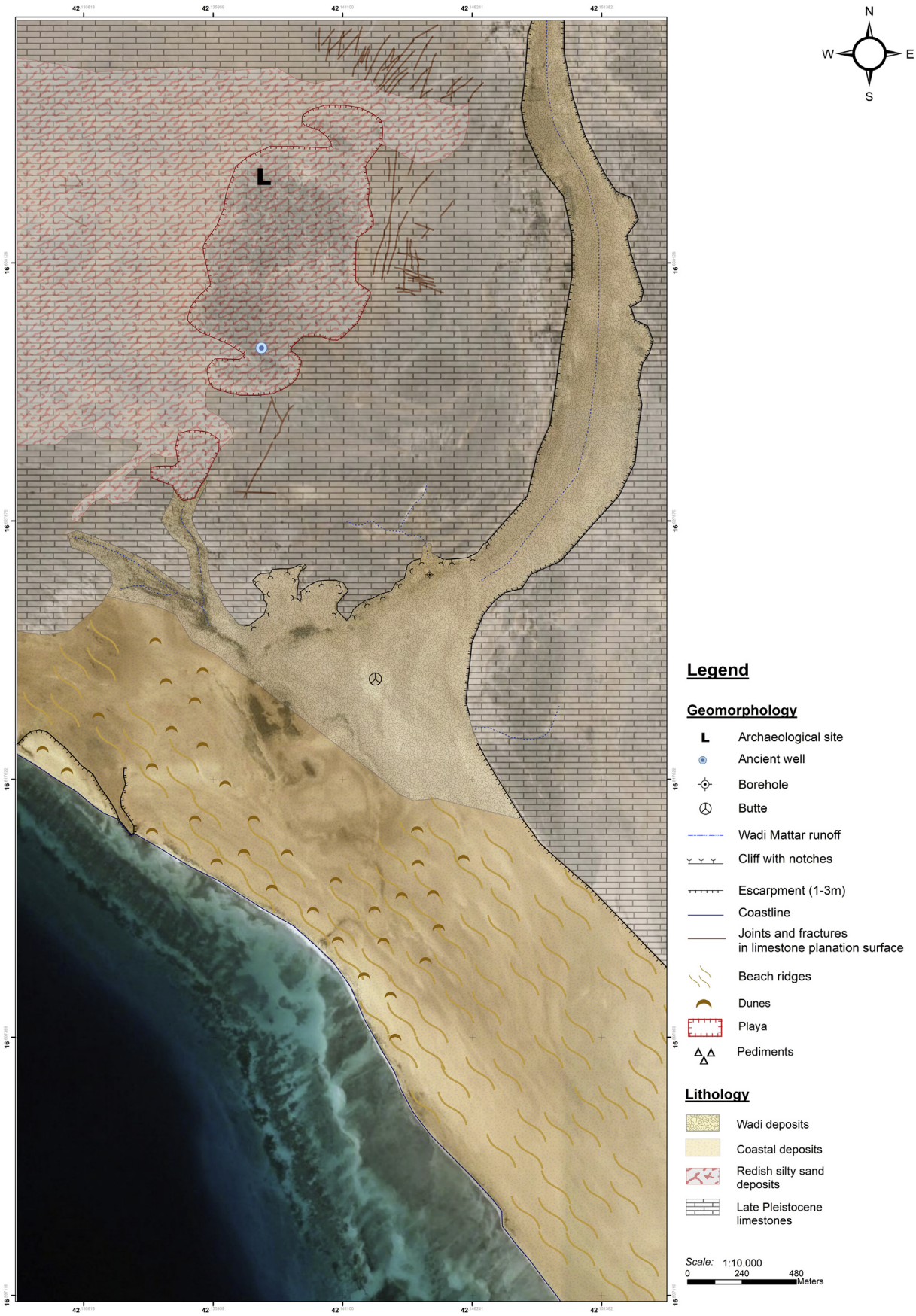

Fig. 2. Geomorphological Map of the study area.

Fig. 3. Archaeological site excavations in the carbonate plateau (a,b). Ancient anchor and well in the surrounding area of the archaeological site (c,d). Uplifted wave cut platform with notches (e). The carbonate plateau consisting of coral reef limestones with lineaments-fractures (f). Coring and sampling by auger equipment (g.h).

analysis. Each sample (10 g dry weight) was treated with H_2O_2 to remove the organic matter, washed through 63 μm sieve, and dried at 70 °C. A subset containing at least 200 benthic foraminifera for each sample was obtained using an Otto microsplitter. The microfauna were identified under Leica APO S8 stereoscope. A scanning electron microscope analysis (SEM Jeol JSM-840A, School of Geology, Aristotle University of Thessaloniki) has been used for taxonomical purposes. The taxonomy of benthic foraminifers was based on Loeblich and Tappan (1987), Hottinger et al. (1993), Abu-Zied et al. (2011) and Dimiza et al. (2016). Over than forty foraminiferal species were identified and foraminiferal density (forams/g) was calculated. Benthic foraminiferal assemblages of the studied core samples were generally rich, but a lot of broken specimens were observed. Although the damaged foraminifera were not including in the counting, the broken-reworked ratio [(broken-reworked specimens/undamaged specimens + broken-reworked specimens)*100] was calculated.

Four samples consisting of marine gastropods shells were collected from the core at depths of 1.10–1.18 m (Cerithiidae), 1.18–1.24 m (Cerithiidae), 2.35–2.40 m (Cerithiidae) and 3.10–3.15 m (Strombidae) for AMS radiocarbon dating. The analysis, accredited to ISO/IEC 17025:2005 Testing Accreditation PJLA #59423 standards, was carried out in Beta Analytic Inc.

4. Results

4.1. Modern landforms

The modern landscape of the Wadi Matar site is characterized by a carbonate plateau consisting of coral reef limestones (Figs. 2 and 3f). The altitude ranges from 10 to 11 m above mean sea level and the slope does not exceed 0.1%. Two major systems of lineaments-fractures are observed on the dissected tableland. The first system is developed with a general direction NW-SE, the same as that detected in the Qumah island (Almalki et al., 2015), dipping to the west (318°/70°, 288°/86° and 245°/65° field measurements). The second system is directed N-S dipping to the NNE (4°/60° field measurements). The carbonate surface is being continuously denuded and exfoliated under subaerial arid conditions forming locally pan-like depressions, namely playas. In addition, few karstic depressions, known as cavernous or honeycomb weathering (Mandurah and Aref, 2012; Bantan et al., 2015; Almalki and Bantan, 2016), have been identified covered by a thin (< 0.5 m) residual soil. A well is located 900 m south of the archaeological site. It

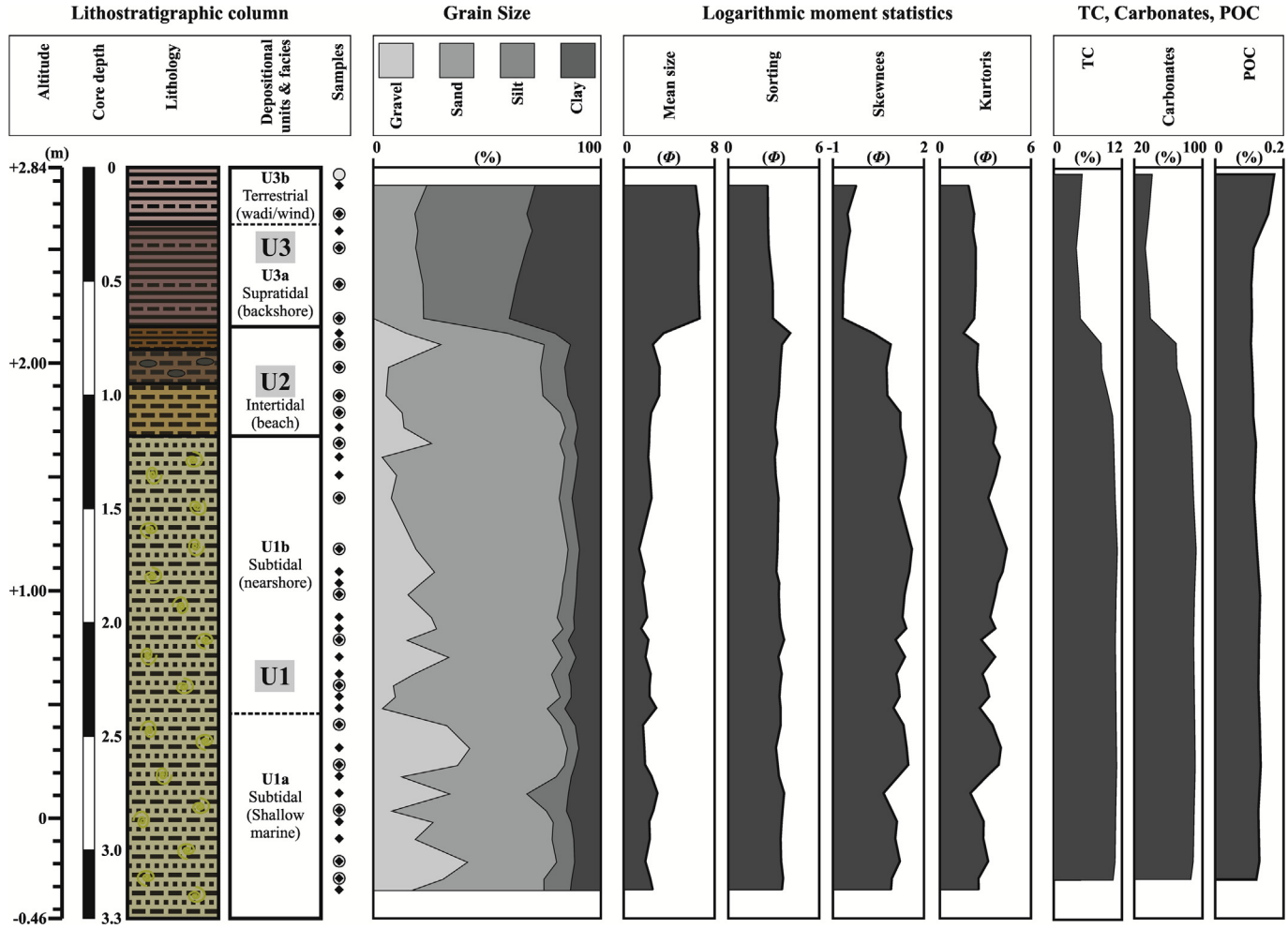

Fig. 4. Granulometry of the borehole Matar-1.

is 7.80 m deep, drills the reefal limestone, and its paved bottom is 1.14 m above the mean sea level (Fig. 3d). At edge of the carbonate platform there are escarpments of 1–3 m high, which are undercut near the beach in the southern part of the mapped area. In some steep escarpments well developed notches are observed (Figs. 2 and 3e).

Pediments at the base of cliffs at both banks of the Wadi Matar valley. The Wadi Matar valley is directed NE-SW, bounded by steep banks and covered by coarse grained sediments. Some alluvial fans are located from both sides of the Wadi Matar valley formed by the sporadic runoff of the carbonate plateau. A butte-like landform is also detected to the southwest of the Wadi Matar valley. The main coastal landforms are the beach ridges consisting of recent coarse grained sediment (sand and gravel) with shells, and the dune fields located on the backshore zone. The extended development of ridges and dunes implies an intense regime of waves and winds that affect significantly the sedimentation pattern of the coastal area.

4.2. Core stratigraphy

4.2.1. Grain size and statistics

The lowest unit of the core Matar-1 (U1, at depths of 1.18–3.30 m) (Fig. 4) consists of two subunits; the subunit U1a (at depths of 2.40–3.30 m) comprises yellow gray, gravelly muddy Sand (gmS) and muddy sandy Gravel (msG) with presence of mollusk fragments. The average contents of gravel (G′), sand (S′), silt (Z′) and clay (C′) fractions are 27.1 ± 11.7%, 51.2 ± 11.3%, 9.0 ± 3.9% and 12.6 ± 1.5%, respectively; while the mean size of particles (x_φ) is 2.240 ± 0.394 φ. The logarithmic moment statistical analysis shows that sediments are very poorly sorted (σ_φ = 3.459 ± 0.160 φ), very fine skewed ($Sk\boldsymbol{\varphi}$ = 1.112 ± 0.246 φ) and very platykyrtic to leptokyrtic (K_φ = 2.999 ± 0.612 φ). The subunit U1b located at depths from 1.18 m to 2.40 m comprises yellowish gray, slightly gravelly muddy Sand ((s)gmS), gravelly muddy Sand (gmS) and muddy sandy Gravel (msG) with existence of many complete and broken shells. Although the percentage of G′ and Z′ is lower (i.e., 16.9 ± 9.1% and 6.1 ± 0.9%, respectively) and C′ is almost equal (i.e., 12.3 ± 1.7%) than those of U1a, the mean size is higher (x_φ = 2.071 ± 0.382 φ); this is due to the much higher content of the sand fraction (S′ = 64.7 ± 8.6%). According to the logarithmic moment method, sediments can be characterized as very poorly sorted (σ_φ = 3.340 ± 0.158 φ), very fine skewed ($Sk\boldsymbol{\varphi}$ = 1.299 ± 0.172 φ) and platykyrtic to very leptokyrtic (K_φ = 3.464 ± 0.508 φ).

The sedimentary unit lying at depths of 0.70–1.18 m (U2) (Fig. 4) contains brown (0.70–0.80 m), reddish brown (0.80–0.95 m) and yellowish brown (0.95–1.18 m) with white mottles, gravelly muddy Sand (gmS). The mean size is 2.833 ± 0.491 φ, the granulometric fractions are 27.1 ± 11.7% for G′, 51.2 ± 11.3% for S′, 9.0 ± 3.9% for Z′ and 12.6 ± 1.5 %for C′, the sorting is 3.438 ± 0.358 φ (extremely poorly and poorly sorted), the skewness is 0.871 ± 0.340 φ (very fine and fine skewed) and the kyrtosis is 2.684 ± 0.765 φ (very platykyrtic, platykyrtic and leptokyrtic).

The uppermost unit of the core (Fig. 4) (U3, at depths of 0–0.70 m) can be distinguished in two sub-sections the U3a, at depths of 0.25–0.70 m, and the U3b, at depths of 0–0.25) m. U3 consists of reddish brown with mottles (0.40–0.70 m) sandy Mud (sM). G′ is absent, while the rest fractions are very different compared to the lower units,

since S′ is 20.5 ± 1.7% for U3a and 20.8 ± 3.7% for U3b, Z′ is 44.3 ± 6.0% for U3a and 48.6 ± 1.1% for U3b, and C′ is 35.3 ± 4.5% for U3a and 30.9 ± 2.5% for U3b. Moment statistics of U3a are 6.590 ± 0.083 φ for mean size, 2.789 ± 0.167 φ for sorting (very poorly sorted), −0.587 ± 0.115 φ for skewess (very coarse and coarse skewed), and 2.280 ± 0.089 φ for kyrtosis (platykurtic), while for U3b are 6.495 ± 0.212 φ for mean size, 2.599 ± 0.011 φ for sorting (very poorly sorted), −0.376 ± 0.214 φ for skewess (coarse skewed and symmetrical), and 2.063 ± 0.266 φ for kyrtosis (very platykurtic and platykurtic).

4.2.2. Total carbon (TC), particulate organic carbon (POC) and carbonate contents

The TC concentration is very high in the lowest unit U1 (Fig. 4) with the average values to be 10.85 ± 0.23% (10.83 ± 0.25% for U1a and 10.87 ± 0.21% for U1b). In U2 the TC decreases considerably from 10.36% at the core depth of 1.10–1.18 cm to 8.33% at the core depth of 0.73–0.80 cm, while in the upper unit U3 it is relatively low (≤4.98%) with the average values to be 4.33 ± 0.36 in U3a and 4.73 ± 0.34% in U3b.

The POC content is very low throughout the core (0.123 ± 0.017%) (Fig. 4). In the two lower units, the POC values are almost stable, while in the uppermost U3 a slight increase is observed from 0.112% at the core depth of 0.30–0.40 cm to the maximum value (0.173%) at the top of the core (depth of 0–0.15 cm).

Carbonates follow similar trend with the TC concentration; that is very high and almost stable values in U1 (89.32 ± 1.88%), diminishing percentage in U2 (75.49 ± 8.10%) and relatively low content in U3 (36.67 ± 2.86%).

4.2.3. Mineralogical composition

X-ray diffraction analysis reveals that the lower unit U1 is dominated by carbonate minerals. The variation of calcite is more or less stable, while high Mg-calcite and aragonite slightly decrease towards the top of U1 (Fig. 5). Although the presence of dolomite decreases from the base of the core to the depth of 1.85–1.90 m, an inverse trend is established in the upper part of U1b. The non-carbonate minerals are of minor importance including mainly quartz, K-feldspar, plagioclase, pyrite, sulfur and halite. Locally, the presence of some minerals become higher, such as quartz at core depths of 3.10–3.15 m and 2.05–2.10 m, K-feldspar at depth of 3.10–3.15 m, gypsum at depth of 2.60–2.65 m, and amphibole at depth of 2.05–2.10 m. Clay minerals are negligible in the lowest units, except at the base of the core (depth of 3.10–3.15 m) where traces of illite and mica, chlorite and kaolinite are determined (Fig. 5).

In the U2 the carbonate minerals remain dominant (Fig. 5), although their occurrence is apparently not as much of that in the lowest units. Calcite progressively increases upwards, high Mg-calcite and aragonite drastically decrease, and dolomite becomes abundant. The presence of non-carbonate minerals is more significant than that of the U1. Quartz, K-feldspar, plagioclase, gypsium, sulfur and clay minerals (mainly, montmorillonite, chlorite and kaolinite) are detected everywhere in the U2, while pyrite shows a continuous decrease towards the top of unit.

In U3 the carbonate minerals are represented mainly by calcite and dolomite, since high Mg-calcite and aragonite can not be detected in XRD diagrams (Fig. 5). The prevailing non-carbonate mineral is the quartz followed by plagioclase and, to a lesser extent, K-feldspar, while clay minerals have a remarkable presence including mica, montmorillonite, chlorite, kaolinite and palygorskite. In addition, evaporites.

4.2.4. Elemental geochemistry

The Al concentration ranges from 0.36% (at the depth of 2.80–2.85 m) to 5.56% (at the depth of 0.30–0.40 m), with the average content to be 1.74 ± 1.92% (Fig. 6a). In the lowest unit of core (i.e., at depths from 1.18 m to 3.30 m), Al presents minimal values (< 0.74%), with its vertical variation to be almost constant. In the U2, Al values show an upwards increase from 0.62% to 1.86% (Fig. 6a). In the uppermost unit U3, Al has values higher than 4.59% and 4.35% with a relatively decreasing trend towards the top. Apart for Ca and S, the rest major elements (i.e., Fe, K, Mg, Mn, Na, P, Si and Ti) present similar trend to Al. Fe ranges from 0.37% to 4.22% with the average concentration to be 1.57 ± 1.50%; K varies between 0.12% and 1.81% having a mean value of 0.60 ± 0.62%; Mg content fluctuates from 1.65% to 4.76% with an average of 2.76 ± 1.23%; the mean Na concentration is 0.68 ± 0.35% with the minimum (0.39%) and maximun (1.32%) measures to occur at the core depths of 1.85–1.90 m (in U1b) and 0.15–0.25 m (in U3b), respectively; the extreme values of P are

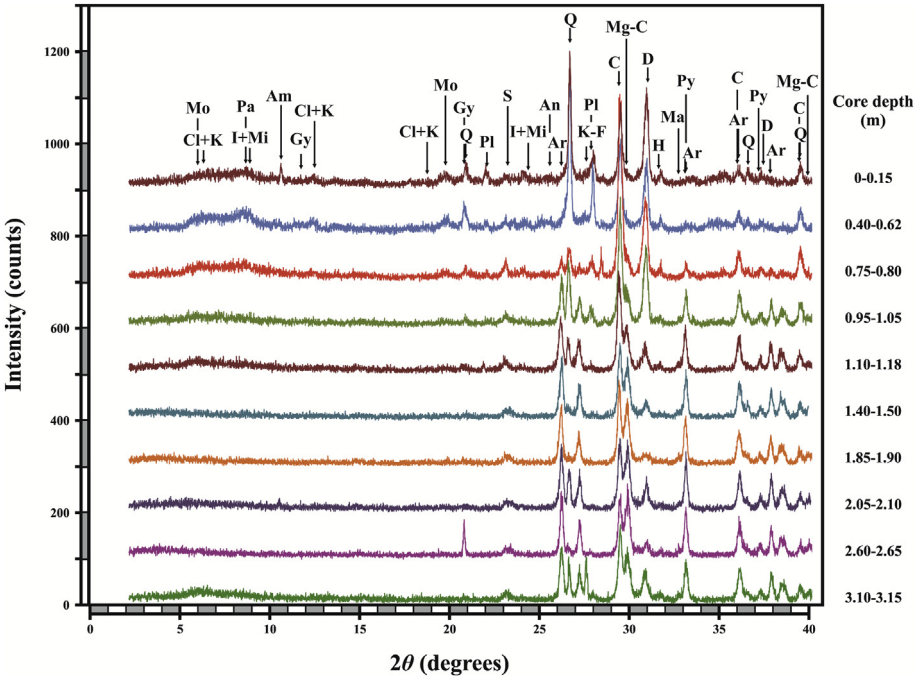

Fig. 5. Mineralogical composition of the samples taken from Borehole Matar-1.

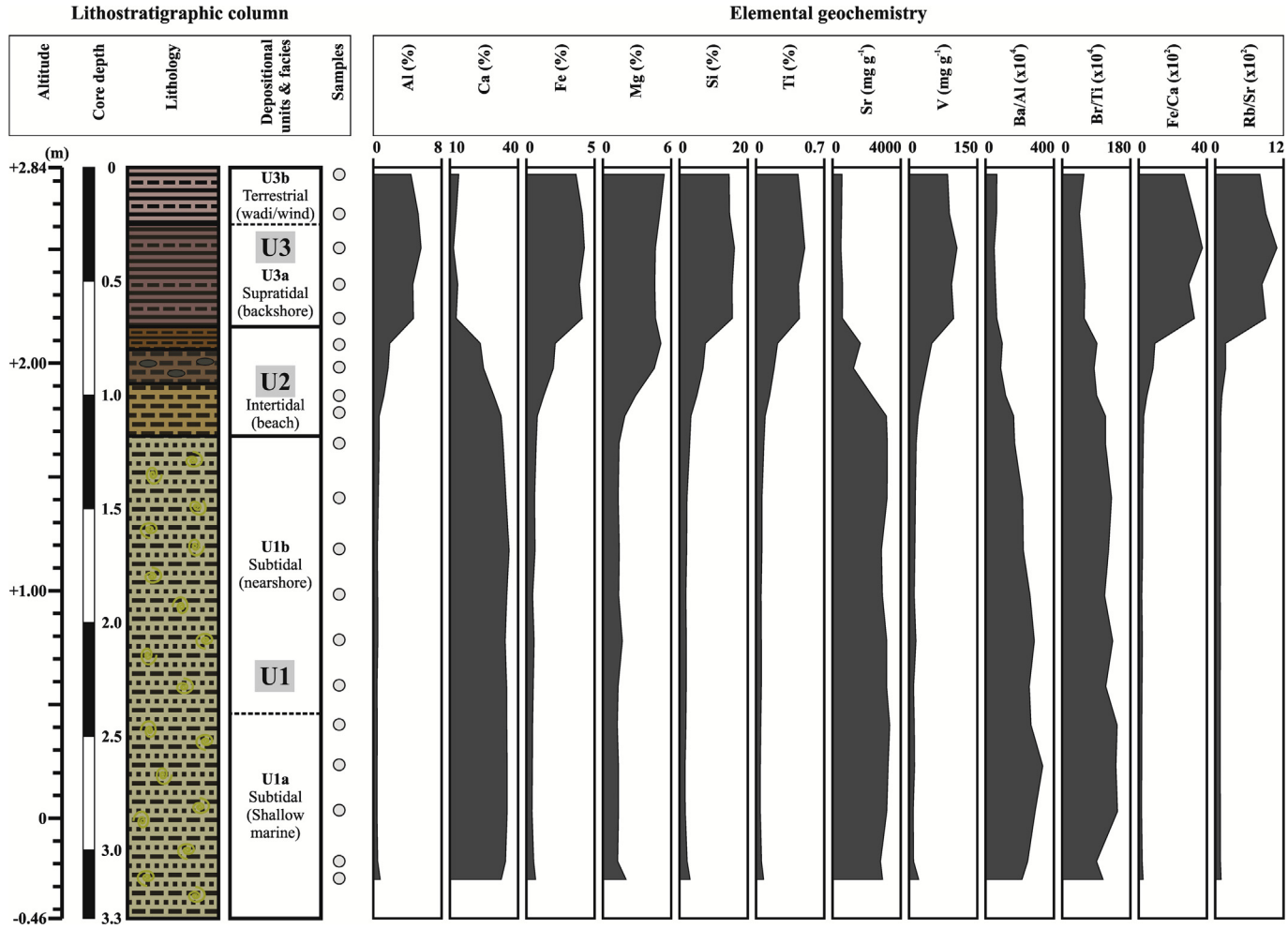

Fig. 6. A: Elemental Geochemistry of the samples from borehole Matar-1.
6b: Elemental Geochemistry of the samples from borehole Matar-1, continue.

0.034% and 0.079%, while the average is 0.05 ± 0.01%; finally, Si and Ti contents obtain the highest values (16.1% and 0.497%, respectively) in the U3a at depths of 0.30–0.40 m, while the lowest values (1.48% and 0.035%, respectively) are recorded in the U1 at depths of 2.60–2.65 m for the Si and 2.80–2.85 m for Ti.

The vertical distribution of Ca concentration shows an opposite trend to the above elements (Fig. 6a). In U1 the values are always higher than 32.4% with the maximum (35.9%) to be determined at the depth of 2.60–2.85 m. In U2, there is a decrease of Ca percentage from the base (32.4%) to the top (23.2%) of the unit. Low measurements (less than 13.7%) are recorded in U3 without any well-established trend.

S concentration does not follow the trend of any of the aforementioned chemical elements. There is a high variability of S values in all units, although the lowest of them (0.036% and 0.060%) occur in the surficial unit of the core (Fig. 6b).

The distribution of trace elements concentration along the core Matar-1 follows three distinct patterns.

The majority of them, i.e. Ba (119.2 ± 88.4 mg kg^{-1}), Br (15.99 ± 5.94 mg kg^{-1}), Co (7.36 ± 6.35 mg kg^{-1}), Cr (40.17 ± 26.69 mg kg^{-1}), Cu (20.57 ± 20.17 mg kg^{-1}), Mn (739.9 ± 632.1 mg kg^{-1}), Mo (3.30 ± 1.33 mg kg^{-1}), Ni (17.86 ± 16.77 mg kg^{-1}), Pb (2.46 ± 2.42 mg kg^{-1}), Rb (28.12 ± 9.31 mg kg^{-1}), V (4.30 ± 0.84 mg kg^{-1}), Y (9.71 ± 7.25 mg kg^{-1}), Zn (59.28 ± 54.86 mg kg^{-1}) and Zr (50.34 ± 49.17 mg kg^{-1}), presents a trend similar to that of Al, Fe, K, Mg, Mn, Na, P, Si and Ti (Fig. 6a and b).

Sr concentration follows a similar pattern to Ca with the higher values (2774.2–3318.6 mg kg^{-1}) to be recorded in unit U1 and the lower (435.0–531.3 mg kg^{-1}) to be determined in U3.

The rest measured trace elements, i.e. As, Ce, I, La and Nb do not show any well defined trend either along the core or within each unit separately. The average value of those elements is: 10.47 ± 2.03 mg kg^{-1} for As, 26.18 ± 11.27 mg kg^{-1} for Ce, 9.09 ± 2.85 mg kg^{-1} for I, 10.42 ± 5.81 mg kg^{-1} for La, and 101.64 ± 5.47 mg kg^{-1} for Nd (Fig. 6b).

4.2.5. Benthic foraminiferal assemblages

In the unit U1a foraminiferal fauna is principally represented by *Ammonia convexa* (34.3 ± 6.3%), *Neorotalia calcar* (11.0 ± 2%) and *Peneroplis* spp. (2.4 ± 0.9%) (Figs. 7 and 8). The total assemblage is completed by more than 15 miliolid species (35.7 ± 7.8%), 9 rotaliid species (4.2 ± 1.5%) and *Elphidium* spp. (11.11 ± 2.5%). The presence of few bolivinid species (mainly *Bolivina spathulata* and *Bolivina striatula)* constantly diminishes towards the top of the unit. The ratio of complete to broken-reworked tests is relatively low (17.4 ± 2.1), while the density ranges between 139 and 626 speciments/g. In the subunit U1b (Fig. 7), the foraminiferal assemblage is mainly formed by *N. calcar* (15.2 ± 6.3) and *A. convexa* (37.32 ± 4.5%); small rotaliids (4.2 ± 3.2%), *Peneroplis* spp. (1.9 ± 2.4%) and miliolids (24.5 ± 3.5%) are present with fluctuating percentages. Foraminiferal density reaches high values (249–603 specimens/g) and broken-reworked tests ratio ranges between 16.1 and 39.4.

The Unit U2 (Fig. 7) benthic foraminiferal assemblage presents

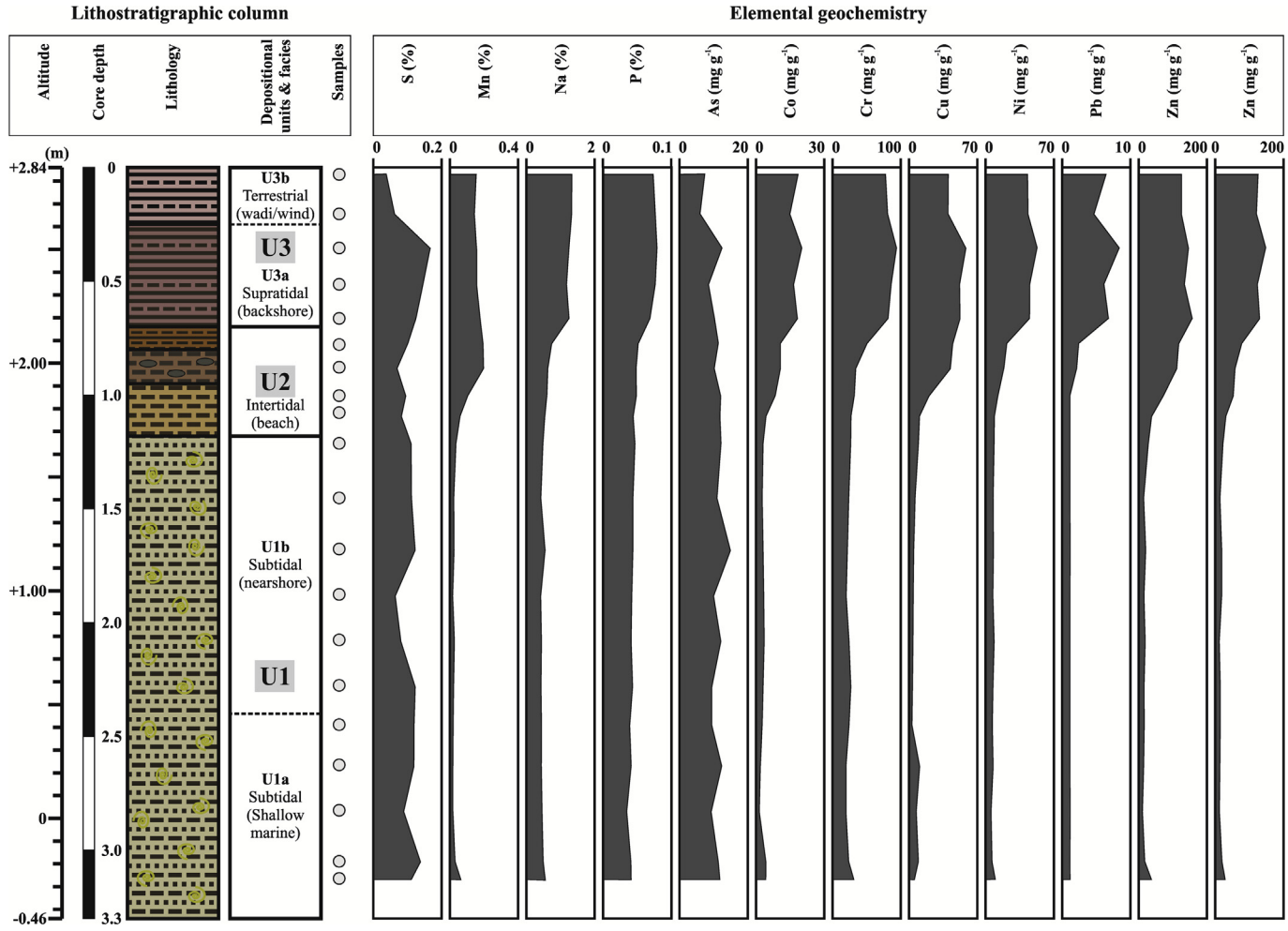

Fig. 6. (*continued*)

similar composition and abundance to the previous Unit U1, while the broken-reworked ratio and foraminiferal density are ranging from 35.4 to 47.4 and from 99 to 124 specimens/g, respectively.

The U3 is characterized by the total absence or very rare appearance of mainly *A. convexa* and small rotaliids. Broken-reworked ratio reaches high values (76.8 ± 7.2), whereas specimens density is very low (5–19 specimens/g). In the uppermost subunit U3b, benthic foraminifera are totally absent (Fig. 7).

4.2.6. Radiocarbon dating

The oldest age has been recorded at the base of the core (U1) and is 5253 ± 223 y cal BP. Two other datings have been performed in the U1b revealing that the age of its base and top is 3675 ± 215 y cal BP and 3138 ± 223 y cal BP, respectively. Finally, the base of the U2 is dated to 3040 ± 220 y cal BP. It is highlighted that no certain information about the relative sea level changes can be extracted by these datings, since they have not carried out on sea level markers, as well as there is a disparity between time of organism death and deposition of its skeleton (Roy, 1991; Woodroffe et al., 2007). The dating of unit U3 has not been conducted because the sediment is transported and reworked.

5. Discussion

5.1. Modern geomorphological processes

The most extended landform of the mapped area is the coral reef plateau. According to Almalki et al. (2015), Bantan et al. (2015), Almalki and Bantan (2016) and Manaa et al. (2016), this tableland has been formed during the MIS 5e (about 122–119 ka BP), and nowadays is situated at the altitude of 10–11 m above mean sea level. The area is uplifted by the combination of tectonics and salt dome diapirism and, therefore, a system of lineaments-fractures is developed on the ground surface. These joints have been detected in many parts of the Farasan Islands (Almalki et al., 2015; Sakellariou et al., 2015; Almalki and Bantan, 2016; Augustin et al., 2016) and the Red Sea, such as Khilah area in Farasan Al Kabir island, Sajid island, Qumah island of the Red Sea (Almalki et al., 2015; Sakellariou et al., 2015; Almalki and Bantan, 2016; Augustin et al., 2016).

The plateau surface undergoes “cavernous or honeycomb weathering” (Almalki and Bantan, 2016), forming karstic depressions, which favours the formation of the playas, since these very shallow basins collects occasionally water forming a temporary lake (Mandurah and Aref, 2012).

At the plateau margin, escarpments have been resulted by erosion during wadi flash flood events and breakdown during arid conditions. The cliff undercuts at the southern edge of the plateau probably correspond to Late Holocene uplifted notches (Gvirtzman, 1994; Mandurah and Aref, 2012).

A butte is also detected to the southwest of the Wadi Matar valley, as remnant of past coastal erosion, when the sea level, at 119–122 ky BP (upper parts of the terraces), was approximately at 5–6 m above its present position (Murray-Wallace and Woodroffe, 2014; Bantan et al., 2015; Manaa et al., 2016).

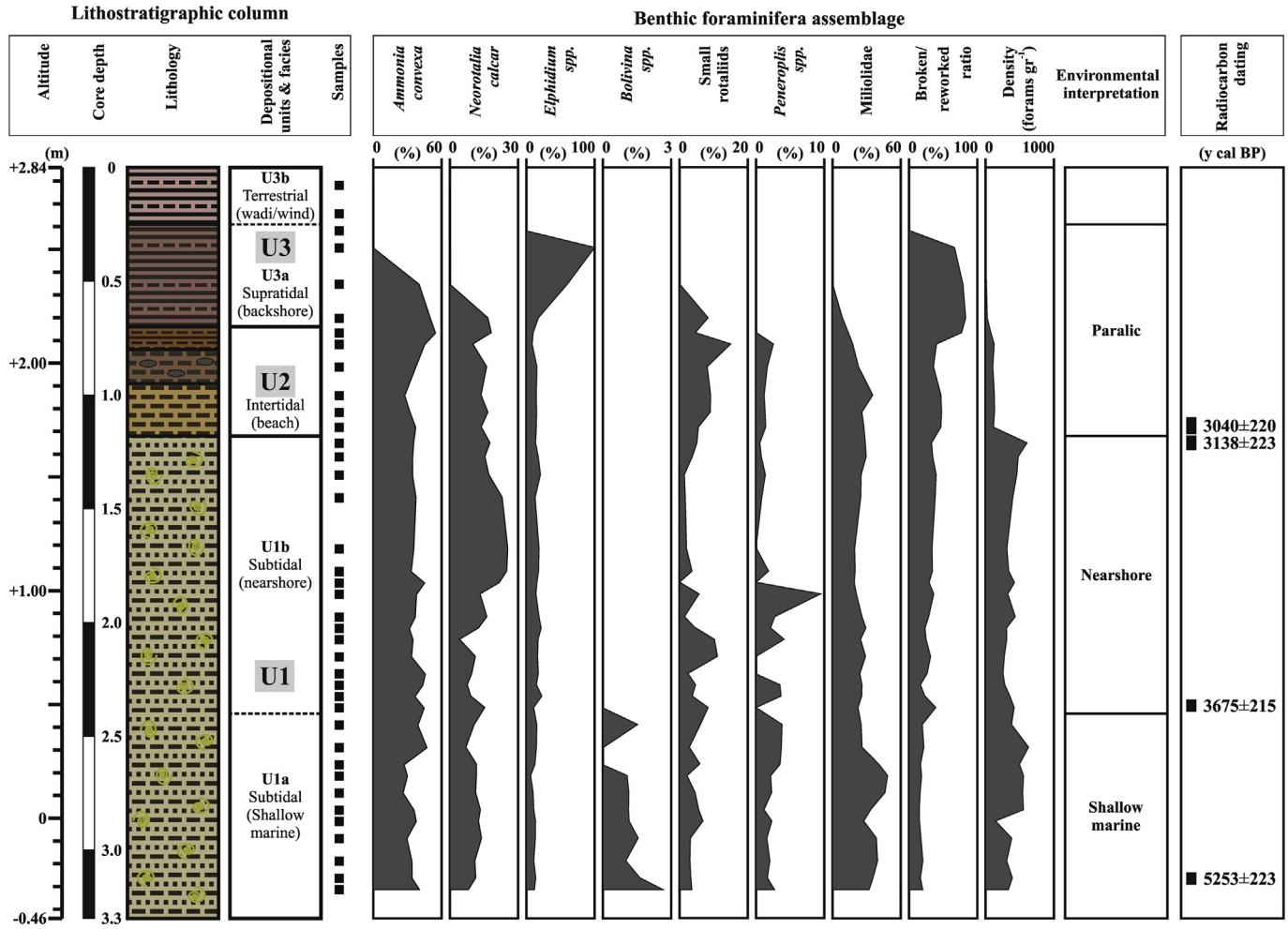

Fig. 7. Foraminiferal assemblages.

5.2. Geomorphological evolution since mid Holocene

The major lithological units are determined on the basis of macroscopic observation (i.e. sedimentary texture, colour and macro fossil occurrence), grain size parameters, organic and inorganic carbon content, mineralogical composition, elemental geochemistry, and benthic foraminiferal assemblages. The lowest U1 is located at depths of 1.18–3.30 m beneath the ground surface; the U2 lies in depths of 0.70–1.18 m; and, the U3 is found at depths of 0 m and 0.70 m.

The texture of sediment composing the lowest subunit of the core (U1a) is biogenic gravely muddy Sand (gmS) and muddy sandy Gravel (msG), while the granulometric type is characterized as bi-/ trimodal, very poorly sorted and very fine skewed. The mud- and sand-sized material consists mainly of corals, molluscs, calcareous algae and benthic foraminifera. In particular, the composition, density and presence of broken or reworked benthic foraminiferal species indicate that a shallow marine environment with relatively high hydrodynamic conditions has been established at least during 5253 ± 223 cal y BP, which subsequently obtains the characteristics of nearshore environment in 3675 ± 215 cal y BP. The presence of large complete or broken shells of molluscs confirms the aforementioned interpretation implying also a subtidal depositional setting, since these gravel-sized fossils can be accumulated *in situ* or transported to the shallow water and/or nearshore areas by local currents (Bantan and Abu-Zied, 2014). The carbonate content is very high (> 85%) and constitutes the main compound of aragonite, high Mg-calcite calcite and dolomite. Variations of the proportion between the above minerals are usually associated with the differences in composition of carbonate-producing organisms; for instance high Mg-calcite is dominant in calcareous red algae, benthic foraminifera, echinoids and bryozoans, while aragonite prevails in green algae, molluscs and coral fragments (Chave, 1962; Chave et al., 1972; Durgaprasada Rao and Behairy, 1986). These differences are caused by changes in hydrographic/ oceanographic conditions, such as seawater temperature, salinity, sunlight transmission, dissolved oxygen availability and circulation pattern, as well as in geomorphological setting including relative sea level fluctuations and detrital sediment supply (Alsharhan and Kendall, 2003). The non-carbonate content is very low consisting mainly of quartz, alkali feldspars, plagioclase, pyrite and sporadically gypsum. Geochemical proxies, e.g. low Fe/Ca, low Rb/Sr, high Ba/Al and high Br/Ti, certify the restricted presence of terrigenous sediment delivery throughout the unit, except the sediment deposited around 5253 ± 223 cal y BP, where a slightly increased amount of detrital material has been added, as indicated also from the relatively increased appearance of quartz, K-feldspars and clay minerals. This enhanced input of terrestrial debris into the shallow marine environment is probably related to the humid period established in North Africa and Saudi Arabia between 5 ka BP and 8 ka BP (Glennie et al., 1994; Moustafa et al., 2000). The subsequent period is characterized by arid conditions, with the maximum aridity to be recorded from 3.3 ka BP to 4.4 ka BP (Arz et al., 2006; Legge et al., 2006; Edelman-Furstenberg et al., 2009; Biton et al., 2010), which favor the carbonate sedimentation. The accumulation rate of bioclastic sediments is 0.48 mm y^{-1} and can be considered as relatively low in comparison to other platform reefs, such as in North Queensland (Hopley et al., 1983), Gulf of Aqaba in Red Sea (Schuhmacher et al., 1995), Lord Howe Island, Tasman Sea (Kennedy and Woodroffe, 2000), and Palau Islands,

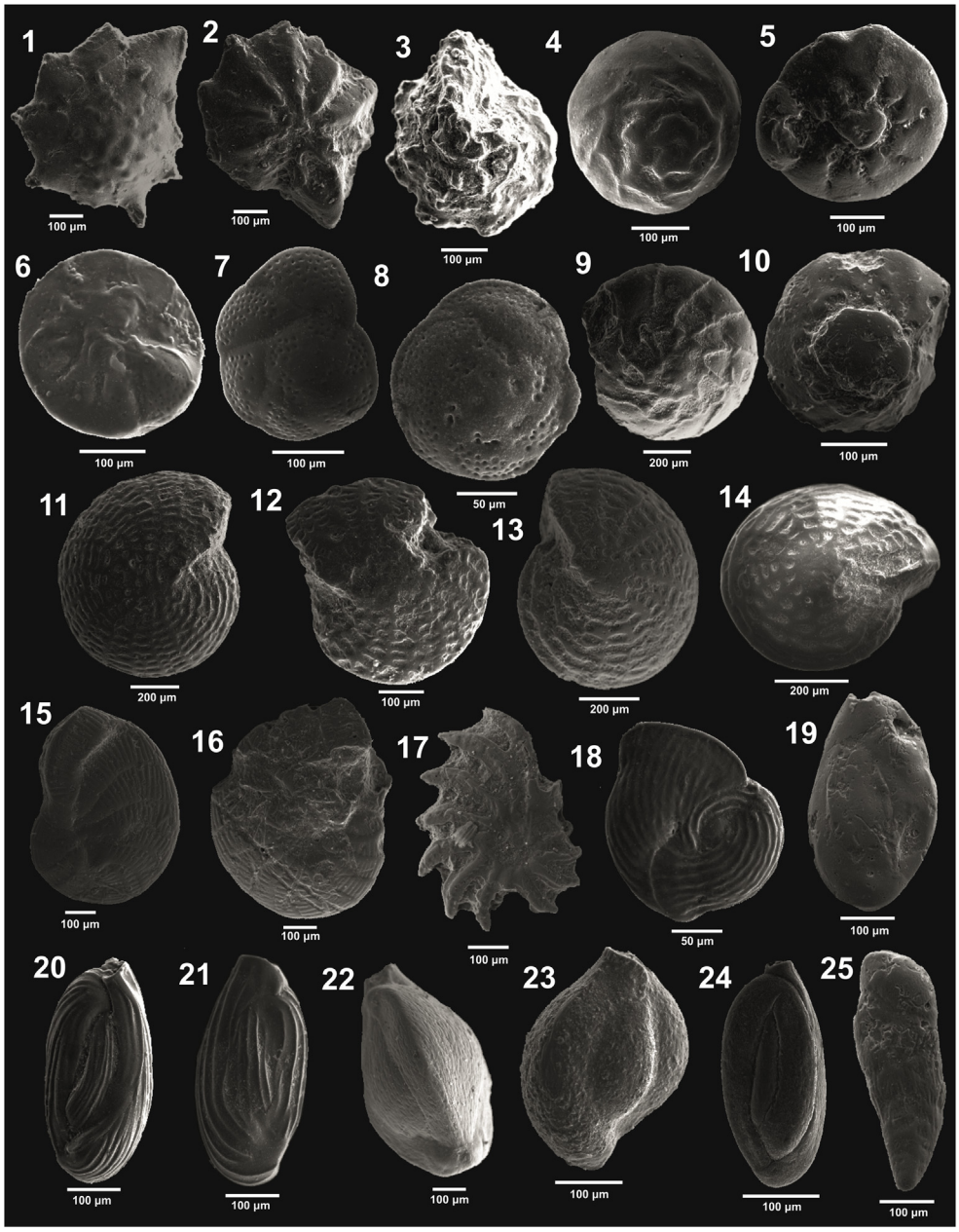

Fig. 8. 1–3 *Neorotalia calcar* (d' Orbigny); 1 spiral view; 2 umbilical view; 3 umbilical view (reworked). 4–5 *Ammonia convexa* (Collins); 4 spiral view. 5 umbilical view; 6 *Neoeponides bradyi* (Le Calvez), umbilical view. 7 *Rosalina floridensis* (Cushman), spiral view. 8 *Rosalina macropora* (Hofker), spiral view. 9–10 *Ammonia convexa* (Collins); 9 spiral view (reworked); 10 umbilical view (reworked). 11–12 *Elphidium striato-puncatum* (Fichtel and Moll); 11 side view; 12 side view (broken).13 *Elphium crispum* (Linné), side view. 14 *Elphidium craticulatum* (Fichtel and Moll), side view. 15–17 *Peneroplis planatus* (Fichtel and Moll); 15 side view; 16 side view (broken); 17 side view (reworked). 18 *Vertebralina striata* d'Orbigny, side view. 19 *Quinqueloculina seminula* (Linné), side view (broken). 20 *Quinqueloculina carinatastriata* (Wiesner), side view. 21 *Quinqueloculina limbata* d'Orbigny, side view. 22 *Triloculina tricarinata* d'Orbigny, side view. 23 *Quinqueloculina lamarckiana* d'Orbigny, side view. 24 *Quinqueloculina stelligera* Schlumberger, side view. 25 *Bolivina striatula* Cushman, side view.

western Pacific (Kayanne et al., 2002). The subunit U1b has been formed between 3138 ± 223 cal y BP and 3675 ± 215 cal y BP, and its physical, chemical and biological characteristics are similar to those of unit U1. However, some differences can be determined, such as the disappearance of the bolivinid species (mainly *Bolivina spathulata* and *Bolivina striatula*) indicating a more sandy substrate and shallower environmental conditions, and the slightly increase of broken forams demonstrating a higher energy regime. The composition and distribution pattern of the foraminiferal assemblage in the U1b presents analogous features to that of Farasan modern nearshore environment (Abu-Zied et al., 2011). Despite that the nearshore setting represents a dynamic environment, a 1.22-m thick reefal sedimentary bed has been accumulated in a period of about 537 years. This average rate (2.17 mm y^{-1}) is 4-fold higher compared to U1a rates and can be attributed to the interplay between the available accommodation space (Kennedy and Woodroffe, 2002) and hydrodynamic factors, such as storm frequency and severity (Braithwaite et al., 2000). Moreover, the topographical irregularities of the reef platform can favor the accumulation of thick bioclastic beds in local depressions, although the area is generally affected by high-energy events (Yamano et al., 2003; Montaggioni, 2005). Arid conditions are still dominant during the formation of U1b with lack of terrestrial material entering into the nearshore zone.

The U2 consists of extremely to very poorly sorted gravely muddy sand (gmS). The analysis of foraminiferal assemblage suggests a transition from the nearshore to paralic (beach) environment starting after 3040 ± 220 y cal BP. The marine species become lesser towards the top of the unit, where up to 50% of them are broken or reworked. For this reason no sampling for dating has been realized in the uppermost part of the core. The total carbonate content diminishes upwards, while the presence of detrital-derived minerals, such as quartz, K-feldspars and plagioclase, increases. Decreasing values of Ca, Sr, Ba/Al and high Br/Ti together with enhancing ratios of Fe/Ca and Rb/Sr indicate that the area is affected by terrestrial processes with greater intensity over the time. The above data suggest that this depositional unit corresponds to a high-energy intertidal environment, where a mixing between marine carbonate and terrestrial siliciclastic end-member materials occurs. The particulate organic carbon does not exceed 0.111% and no

low-energy lagoonal sediment is detected in this unit.

All available data support that the processes formed the unit U3 are different than those of the lower units. The sediment of subunit U3a is fine-grained and can be classified as bimodal, very poorly sorted sandy mud (sM). The ratios of Fe/Ca and Rb/Sr are high, indicating a significant input of detrital material. The dominant minerals are quartz, feldspar and clay minerals with considerable amount of carbonate (mainly, calcite and dolomite) and evaporate (mainly, anhydrite, gypsum and halite) minerals. This mineral suite demonstrates a supratidal environment, which is affected sporadically by storm events. The marine foraminiferal specimens are rare and only 5 different species with low absolute abundance (density of 0–20 specimens/g) are recognized. The majority of their tests (up to 75%) are broken, and therefore, they can be considered as transported. Since no certain *in situ* test has been found, no dating from this unit has been achieved. The surficial subunit U3b has almost the same composition and characteristics with the U3a. However, the main difference is the absence of foraminiferal species; this means that there is no influence of marine processes on the area. The material should be supplied by both Wadi Matar flood flashes and/or aeolian process. Wadi Matar drains the reefal limestone of southern part of Farasan Al Kabir Island and carries to the study area mainly bioclastic debris (Bantan, 1999). In addition, strong winds transfer dust from the adjacent (African and Arabian Peninsula) deserts covering large parts of the Farasan archipelago (Basaham et al., 2014). Finally, diagenetic evaporite crystals are formed in the matrix of mechanically deposited carbonate or siliciclastic material, without developing any distinct layer. Nevertheless, the thickness of interval remains small (about 0.25 m), due to the wadi and wind reworking effects that erode and remove the initially deposited material. Therefore, no dating has been realized in this transported and heavily reworked material.

The core Matar-1 provides a complete sequence since mid Holocene from the southern coast of the Farasan Al Kabir Island including a succession of subtidal, intertidal, supratidal and wadi/aeolian depositional pattern. In general, this stratigraphic sequence follows the Holocene sea-margin sabkha depositional model of the southern Arabian Gulf described by Warren (1991). This Holecene depositional pattern is associated with the progressive reduction of the accommodation space caused by the combination of sea level change (Lambeck et al., 2011), infilling by sediment (Bantan and Abu-Zied, 2014) and diapir uplift (Almalki et al., 2015). The subtidal reflects deposition in the high-energy shallow marine section of a reefal platform which, over the time, becomes the shallower nearshore part of the reef ramp. The intertidal facies reveals a beach setting with an intensive hydrodynamic regime that transports and reworks both biogenic and terrigenous sand. The supratidal and wadi/aeolian facies are affected mainly by terrestrial processes, mostly driven by the Wadi Matar runoff and the wind activity.

The aforementioned paleo-environmental evolution is in accordance with the results of recent geoarchaeological surveys focused on the distribution of shell-midden sites in Farasan Islands. Since shell-middens are located very close and almost parallel to sandy or rocky shores of shallow marine basins, they are used as indicators for the reconstruction of paleo-landscapes (Bailey et al., 2013; Meredith-Williams et al., 2014). In the south Al Kabir Island the cluster of shell mounds is traced in the vicinity of the reefal-limestone platform edge situated at the southeast of the sampling position. Since the accumulation of mounds has been dated to about 5000–5500 y cal BP, the drilling area should be a shallow marine platform at the same time. The above reasonable association is confirmed by the facies characteristics of the basal Matar-1 unit. Subsequently, the shallow marine bay is filled by carbonate sediment with the paleo-shoreline being located on the borehole site around 3100 y cal BP. Since then the region received an increasing load of detrial material, which infilled the area and shifted the shoreline towards its present position.

6. Conclusions

The southeast coast of the Farasan Al Kabir Island is formed from uplifted reefal limestone. The arid low-lying topography includes hard rock formations, such as coral limestone plateau, cliffs and pediments, as well as soft-sediment fromations, such as playa-like depressions located on plateau surfaces, alluvial fans and bajada, and sandy beaches. The paleoenvironmental changes of the area since the mid Holocene have been determined by a multiproxy analysis of 3.3-m sediment core. Three depositional units have been recognized suggesting a gradual transition from shallow marine to terrestrial settings. The formation of the lowest unit (U1) dated to mid Holocene represents a relatively high-energy shallow marine bay where carbonate sedimentation is dominant. From 3675 ± 215 y cal BP and till 3138 ± 223 y cal BP, the area receives carbonate sediments (U1b) with the same characteristics with those of the older subunit (U1a), but the environment is changed to a nearshore reef flat. After 3138 ± 223 y cal BP, terrigeous material enters into an intertidal setting, which in particular is defined as a high-energy beach without the presence of any lagoon. Subsequently, mixed terrigenous, carbonate and evaporite sediment is accumulated in a supratidal (backshore) zone of the beach, which later is modified to a terrestrial setting affected by the Wadi Matar and aeolian action.

Acknowledgments

The authors would like to thank Prof. F. Villeneuve and Dr. M. Mouton for their full support and collaboration during the research survey. We are indebted to HRH Prince Sultan Bin Salman Bin Abdulaziz Al Saud (President and Chairman of the Directors Board of the Saudi Commission for Tourism and Antiquities, SCTA), as well as to Dr Al-Saud, Professor Ali Al-Ghabbān (Vice-President of SCTA) and Dr Jamal Al Omar (Director General of SCTA), for granting permission to carry out the fieldwork. We also gratefully acknowledge the cooperation and help of Dr Al-Modare, Dr Mofareh and M. Aqīlī, members of SCTA in Jizān and Farasān. Sincere thanks are also extended to P.-M. Blanc, G. Davtian and C.S. Phillips, for fieldwork assistance as well as A. Papageorgiou, G. Kampouri, A. Androni and I. Stavrakaki, from Hellenic Centre for Marine Research, for performing the laboratory analyses. Finally, the author greatly appreciate the comments of Dr T. Kanellopoulos and Dr J. Panagiotopoulos which highly improved the final version of the manuscript.

References

Abu-Zied, R.H., Bantan, R.A., Basaham, A.S., El Mamoney, M.H., Al-Washmi, H.A., 2011. Composition, distribution, and taphonomy of nearshore benthic foraminifera of the Farasan Islands, southern Red Sea, Saudi Arabia. J. Foraminifer. Res. 41 (4), 349–362.

Al Mutairi, K., El-Bana, M., Mansor, M., Al-Rowaily, S., Mansor, A., 2012. Floristic diversity, composition, and environmental correlates on the arid, coralline islands of the Farasan Archipelago, Red Sea, Saudi Arabia. Arid Land Res. Manag. 26 (2), 137–150.

Alfarhan, A.H., Al-Turki, T.A., Thomas, J., Basahy, R.A., 2016. Annotated List to the flora of Farasan Archipelago, Southern Red Sea, Saudi Arabia, vol. 22 Taeckholmia.

Almalki, K.A., Ailleres, L., Betts, P.G., Bantan, R.A., 2015. Evidence for and relationship between recent distributed extension and halokinesis in the Farasan Islands, southern Red Sea, Saudi Arabia. Arab.J. of Geosci. 8 (10), 8753–8766.

Almalki, K.A., Bantan, R.A., 2016. Lithologic units and stratigraphy of the Farasan islands, southern Red Sea. Carbonates Evaporites 31 (2), 115–128.

Alsharekh, A.M., Bailey, G.N., 2014. Coastal Prehistory in Southwest Arabia and the Farasan Islands: 2004–2009 Field Investigations. Saudi Commission for Tourism and Antiquities, Riyadh.

Alsharhan, A.S., Kendall, C.S.C., 2003. Holocene coastal carbonates and evaporites of the southern Arabian Gulf and their ancient analogues. Earth Sci. Rev. 61 (3), 191–243.

Alwelaie, A.N., Chaudary, S.A., Alwetaid, Y., 1993. Vegetation of some Red Sea islands of the Kingdom of Saudi Arabia. J. Arid Environ. 24 (3), 287–296.

Arz, H.W., Lamy, F., Pätzold, J., 2006. A pronounced dry event recorded around 4.2 ka in brine sediments from the northern Red Sea. Quat. Res. 66 (3), 432–441.

Augustin, N., van der Zwan, F.M., Devey, C.W., Ligi, M., Kwasnitschka, T., Feldens, P., Bantan, R.A., Basaham, A.S., 2016. Geomorphology of the central Red Sea rift: determining spreading processes. Geomorphology 274, 162–179.

Bailey, G.N., Flemming, N.C., King, G.C., Lambeck, K., Momber, G., Moran, L.J., Al-

Sharekh, A., Vita-Finzi, C., 2007. Coastlines, submerged landscapes, and human evolution: the Red Sea basin and the Farasan islands. J. I. Coast Archaeol. 2 (2), 127–160.
Bailey, G.N., 2009. The Red Sea, coastal landscapes, and hominin dispersals. In: Petraglia, M.D., Rose, J.I. (Eds.), The Evolution of Human Populations in Arabia: Paleoenvironments, Prehistory and Genetics. Springer, Netherlands, pp. 15–37.
Bailey, G.N., Meredith-Williams, M.G., Alsharekh, A.M., 2013. Shell mounds of the Farasan islands, Saudi Arabia. In: Bailey, G.N., Hardy, K., Camara, A. (Eds.), Shell Energy: Mollusc Shells as Coastal Resources. Oxbow, Oxford, pp. 241–254.
Bailey, G.N., 2015. The evolution of the Red Sea as a human habitat during the quaternary period. In: Rasul, N.M.A., Stewart, I.C.F. (Eds.), The Red Sea. Springer-Verlag, Berlin Heidelberg, pp. 599–614.
Bailey, G.N., Devès, M.H., Inglis, R.H., Meredith-Williams, M.G., Momber, G., Sakellariou, D., Sinclair, A.G.M., Rousakis, G., Al Ghamdi, S., Alsharekh, A.M., 2015. Blue Arabia: palaeolithic and underwater survey in SW Saudi Arabia and the role of coasts in Pleistocene dispersals. Quat. Int. 382, 42–57.
Bantan, R.A., 1999. Geology and Sedimentary Environments of Farasan Bank (Saudi Arabia), Southern Red Sea: a Combined Remote Sensing and Field Study (Doctoral Dissertation, University of London).
Bantan, R.A., Abu-Zied, R.H., 2014. Sediment characteristics and molluscan fossils of the Farasan Islands shorelines, southern Red Sea, Saudi Arabia. Arab.J. of Geosci. 7 (2), 773–787.
Bantan, R.A., Abu-Zied, R.H., Haredy, R.A., 2015. Lithology, fauna and environmental conditions of the Late Pleistocene raised reefal limestone of the Jeddah coastal plain, Saudi Arabia. Arab.J. of Geosci. 8 (11), 9887–9904.
Basaham, A.S., Gheith, A.M., Khawfany, A.A.A., Sharma, R., Hashimi, N.H., 2014. Sedimentary variations of geomorphic subenvironments at Al-Lith area, central-west coast of Saudi Arabia, Red Sea. Arab.J. of Geosci. 7 (3), 951–970.
Behairy, A.K.A., 1983. Marine transgressions in the west coast of Saudi Arabia (Red Sea) between mid-Pleistocene and Present. Mar. Geol. 52 (1–2), M25–M31.
Bemert, G., Ormond, F.R.G., 1981. Red Sea Coral Reefs. Kegan Paul Internat, London, pp. 192.
Berumen, M.L., Hoey, A.S., Bass, W.H., Bouwmeester, J., Catania, D., Cochran, J.E., Khalil, M.T., Miyake, S., Mughal, M.R., Spaet, J.L.Y., Saenz-Agudelo, P., 2013. The status of coral reef ecology research in the Red Sea. Coral Reefs 32 (3), 737–748.
Biton, E., Gildor, H., Trommer, G., Siccha, M., Kucera, M., Van Der Meer, M.T.J., Schouten, S., 2010. Sensitivity of Red Sea circulation to monsoonal variability during the Holocene: an integrated data and modeling study. Paleoceanography 25 (4) PA4209.
Bos, J.A., Huisman, D.J., Kiden, P., Hoek, W.Z., van Geel, B., 2005. Early Holocene environmental change in the Kreekrak area (Zeeland, SW-Netherlands): a multi-proxy analysis. Palaeogeography, Palaeoclimatology, Palaeoecol. 227 (4), 259–289.
Bosence, D., 2005. A genetic classification of carbonate platforms based on their basinal and tectonic settings in the Cenozoic. Sediment. Geol. 175 (1), 49–72.
Braithwaite, C.J.R., Montaggioni, L.F., Camoin, G.F., Dalmasso, H., Dullo, W.C., Mangini, A., 2000. Origins and development of Holocene coral reefs: a revisited model based on reef boreholes in the Seychelles, Indian Ocean. Int. J. Earth Sci. 89 (2), 431–445.
Bruckner, A., Rowlands, G., Riegl, B., Purkis, S.J., Williams, A., Renaud, P., 2012. Atlas of Saudi Arabian Red Sea Marine Habitats. Khaled bin Sultan Living Ocean Foundation and Panoramic Press, Phoenix, AZ 262 p.
Cann, J.-H., Belperio, A.P., Gostin, V.A., Murray-Wallace, C.V., 1988. Sea-level history, 45,000 to 30,000 yr BP, inferred from benthic foraminifera, Gulf St. Vincent, South Australia. Quat. Res. 29 (2), 153–175.
Cann, J.H., Bourman, R.P., Barnett, E.J., 2000. Holocene foraminifera as indicators of relative estuarine-lagoonal and oceanic influences in estuarine sediments of the River Murray, South Australia. Quat. Res. 53 (3), 378–391.
Cearreta, A., Cachão, M., Cabral, M.C., Bao, R., de Jesus Ramalho, M., 2003. Lateglacial and Holocene environmental changes in Portuguese coastal lagoons 2: microfossil multiproxy reconstruction of the Santo André coastal area. Holocene 13 (3), 447–458.
Chave, K.E., 1962. Factors influencing the mineralogy of carbonate sediments. Limnol. Oceanogr. 7 (2), 218–223.
Chave, K.E., Smith, S.V., Roy, K.J., 1972. Carbonate production by coral reefs. Mar. Geol. 12 (2), 123–140.
Cooper, J.P., Zazzaro, C., 2014. The Farasan Islands, Saudi Arabia: towards a chronology of settlement. Arabian Archaeol. Epigr. 25 (2), 147–174.
da Conceicao Freitas, M., Andrade, C., Rocha, F., Tassinari, C., Munhá, J.M., Cruces, A., Vidinha, J., da Silva, C.M., 2003. Lateglacial and Holocene environmental changes in Portuguese coastal lagoons 1: the sedimentological and geochemical records of the Santo André coastal area. Holocene 13 (3), 433–446.
Dabbagh, A., Hotzl, H., Schnier, H., 1984. Farasan Islands. General considerations and geological structure. In: In: Jado, A.R., Zoti, J.G. (Eds.), Quaternary Period in Saudi Arabia, vol. 2. Springer-Verlag., New Vienna and York, pp. 212–220.
Delagnes, A., Crassard, R., Bertran, P., Sitzia, L., 2013. Cultural and human dynamics in southern Arabia at the end of the Middle Paleolithic. Quat. Int. 300, 234–243.
Dellwig, O., Hinrichs, J., Hild, A., Brumsack, H.J., 2000. Changing sedimentation in tidal flat sediments of the southern North Sea from the Holocene to the present: a geochemical approach. J. Sea Res. 44 (3), 195–208.
Di Rita, F., Simone, O., Caldara, M., Gehrels, W.R., Magri, D., 2011. Holocene environmental changes in the coastal Tavoliere Plain (Apulia, southern Italy): a multiproxy approach. Palaeogeogr. Palaeoclimatol. Palaeoecol. 310 (3), 139–151.
Dias, J.M.A., Boski, T., Rodrigues, A., Magalhães, F., 2000. Coast line evolution in Portugal since the Last Glacial Maximum until present-a synthesis. Mar. Geol. 170 (1), 177–186.
Dimiza, M.D., Koukousioura, O., Triantaphyllou, M.V., Dermitzakis, M.D., 2016. Live and dead benthic foraminifera assemblages from coastal environments of the Aegean Sea (Greece): distribution and diversity. Rev. Micropaleontol. 59, 19–32.
Dinelli, E., Ghosh, A., Rossi, V., Vaiani, S.C., 2012. Multiproxy reconstruction of late pleistocene-holocene environmental changes in coastal successions:microfossil and geochemical evidences from the Po Plain (Northern Italy). Stratigr. 9 (2), 153–167.
Durgaprasada Rao, N., Behairy, A.K.A., 1986. Nature and composition of shore-zone sediments between Jeddah and Yanbu, eastern Red Sea. Mar. Geol. 70 (3), 287–305.
Edelman-Furstenberg, Y., Almogi-Labin, A., Hemleben, C., 2009. Paleoceanographic evolution of central Red Sea during the late holocene. Holocene 19, 117–127.
El Demerdash, M.A., 1996. The vegetation of the farasān islands, Red Sea, Saudi Arabia. J. Veg. Sci. 7 (1), 81–88.
Fabricius, K.E., 2005. Effects of terrestrial runoff on the ecology of corals and coral reefs: review and synthesis. Mar. Pollut. Bull. 50 (2), 125–146.
Folk, R.L., 1974. Petrography of Sedimentary Rocks. Univ. Texas, Hemphill, Austin, Tex 182.
Friedman, G.M., 1968. Geology and geochemistry of reefs, carbonate sediments, and waters, Gulf of Aqaba (Elat), Red Sea. J. Sediment. Res. 38 (3), 895–919.
Fryberger, S., Goudie, A.S., 1981. Arid geomorphology. Prog. Phys. Geogr. 5 (3), 420–428.
Gladstone, W., 2002. Fisheries of the Farasan islands (Red Sea). Naga. World Fish. Cent. Q. 25 (3–4), 30–34.
Glennie, K.W., Pugh, J.M., Goodall, T.M., 1994. Late quaternary Arabian desert models of Permian Rotliegend reservoirs. Explor. Bull. 274, 1–19.
Gvirtzman, G., 1994. Fluctuations of sea level during the past 400 000 years: the record of Sinai, Egypt (northern Red Sea). Coral Reefs 13 (4), 203–214.
Hall, M., Llewellyn, O.A., Miller, A.G., Al-Abbasi, T.M., Al-Wetaid, A.H., Al-Harbi, R.J., Al-Shammari, K.F., 2010. Important plant areas in the Arabian Peninsula: 2. Farasan archipelago. Edinb. J. Bot. 67 (2), 189–208.
Hammond, E.-H., 1954. Small-scale continental landform maps. Ann. Assoc. Am. Geogr. 44 (1), 33–42.
Hausmann, N., Meredith-Williams, M., 2016. Seasonal patterns of coastal exploitation on the Farasan Islands, Saudi Arabia. J. I. Coast Archaeol. 1–20.
Heiss, G.A., 1994. Coral reefs in the Red Sea: Growth, production and stable isotopes (Doctoral dissertation, GEOMAR Forschungszentrum für marine Geowissenschaften).
Hopley, D., Slocombe, A.M., Muir, F., Grant, C., 1983. Nearshore fringing reefs in North Queensland. Coral Reefs 1 (3), 151–160.
Horton, B.P., Culver, S.J., Hardbattle, M.I., Larcombe, P., Milne, G.A., Morigi, C., Whittaker, J.E., Woodroffe, S.A., 2007. Reconstructing Holocene sea-level change for the central Great Barrier Reef (Australia) using subtidal foraminifera. J. Foraminifer. Res. 37 (4), 327–343.
Hottinger, L., Halicz, E., Reiss, Z., 1993. Recent Foraminifera from the Gulf of Aqaba, Red Sea, vol. 179. Slavenska Akademija Znanosti in Umetnosti, Ljubljana, pp. 230.
Karageorgis, A.P., Anagnostou, C.L., Kaberi, H., 2005. Geochemistry and mineralogy of the NW Aegean Sea surface sediments: implications for river runoff and anthropogenic impact. Appl. Geochem. 20, 69–88.
Kayanne, H., Yamano, H., Randall, R.H., 2002. Holocene sea-level changes and barrier reef formation on an oceanic island, Palau Islands, western Pacific. Sediment. Geol. 150 (1), 47–60.
Kennedy, D.M., Woodroffe, C.D., 2000. Holocene lagoonal sedimentation at the latitudinal limits of reef growth, Lord Howe Island, Tasman Sea. Mar. Geol. 169 (3), 287–304.
Kennedy, D.M., Woodroffe, C.D., 2002. Fringing reef growth and morphology: a review. Earth Sci. Rev. 57 (3), 255–277.
Khalil, H.M., 2012. Pliocene-Pleistocene stratigraphy and macrofauna of the Farasan islands, south East Red Sea, Saudi Arabia. Arab.J. of Geosci. 5 (6), 1223–1245.
Klaus, R., 2015. Coral Reefs and Communities of the Central and Southern Red Sea (Sudan, Eritrea, Djibouti, and Yemen). In: Rasul, N.M.A., Stewart, I.C.F. (Eds.), The Red Sea. Springer-Verlag, Berlin Heidelberg, pp. 409–451.
Koukousioura, O., Triantaphyllou, M.V., Dimiza, M.D., Pavlopoulos, K., Syrides, G., Vouvalidis, K., 2012. Benthic foraminiferal evidence and paleoenvironmental evolution of Holocene coastal plains in the Aegean Sea (Greece). Quat. Int. 261, 105–117.
Kraft, J.C., 1971. Sedimentary facies patterns and geologic history of a Holocene marine transgression. Geol. Soc. Am. Bull. 82 (8), 2131–2158.
Lambeck, K., Chappell, J., 2001. Sea-level change through the last glacial cycle. Science 292, 679–686.
Lambeck, K., Purcell, A., Flemming, N.C., Vita-Finzi, C., Alsharekh, A.M., Bailey, G.N., 2011. Sea level and shoreline reconstructions for the Red Sea: isostatic and tectonic considerations and implications for hominin migration out of Africa. Quat. Sci. Rev. 30 (25), 3542–3574.
Legge, H.L., Mutterlose, J., Arz, H.W., 2006. Climatic changes in the northern Red Sea during the last 22,000 years as recorded by calcareous nannofossils. Paleoceanography 21, PA1003.
Loeblich, A.R., Tappan, H., 1987. Foraminiferal Genera and Their Classification. Von Nostrand Reimhold Co, New York 970 pp.
Macfadyen, W.A., 1930. The Geology of the Farsan islands, Gizan and Kamaran island, Red Sea. Geol. Mag. 67 (7), 310–315.
Manaa, A.A., Jones, B.G., McGregor, H.V., Zhao, J.X., Price, D.M., 2016. Dating quaternary raised coral terraces along the Saudi Arabian Red Sea coast. Mar. Geol. 374, 59–72.
Mandurah, M.H., Aref, M.A., 2012. Lithostratigraphy and standard microfacies types of the Neogene carbonates of Rabigh and Ubhur areas, Red Sea coastal plain of Saudi Arabia. Arab.J. of Geosci. 5 (6), 1317–1332.
Mansour, A.M., Madkour, H.A., 2015. Raised coral reefs and sediments in the coastal area of the Red Sea. In: Rasul, N.M.A., Stewart, I.C.F. (Eds.), The Red Sea. Springer-Verlag, Berlin Heidelberg, pp. 379–393.
Marion de Procé, S., Phillips, C., 2010. South Arabian inscriptions from the Farasan

islands (Saudi Arabia). In: In: Starkey, J. (Ed.), Proceedings of the Seminar for Arabian Studies, vol. 40. Archaeopress, Oxford, pp. 277–282.
Meredith-Williams, M.G., Hausmann, N., Bailey, G.N., King, G.C.P., Alsharekh, A., Al Ghamdi, S., Inglis, R.H., 2014. Mapping, modelling and predicting prehistoric coastal archaeology in the southern Red Sea using new applications of digital-imaging techniques. World Archaeol. 46 (1), 10–24.
Montaggioni, L.F., 2005. History of Indo-Pacific coral reef systems since the last glaciation: development patterns and controlling factors. Earth Sci. Rev. 71 (1), 1–75.
Morhange, C., Goiran, J.P., Bourcier, M., Carbonel, P., Le Campion, J., Rouchy, J.M., Yon, M., 2000. Recent holocene paleo-environmental evolution and coastline changes of Kition, Larnaca, Cyprus, Mediterranean sea. Mar. Geol. 170 (1), 205–230.
Moustafa, Y.A., Pätzold, J., Loya, Y., Wefer, G., 2000. Mid-Holocene stable isotope record of corals from the northern Red Sea. Int. J. Earth Sci. 88 (4), 742–751.
Murray-Wallace, C.V., Woodroffe, C.D., 2014. Quaternary Sea-level Changes: a Global Perspective. Cambridge University Press.
Piloyan, A., Konečný, M., 2017. Semi-automated classification of landform elements in Armenia based on SRTM DEM using k-means unsupervised classification. Quaest. Geogr. 36 (1), 93–103.
Pirazzoli, P.A., Pluet, J., 1991. s. World Atlas of Holocene Sea-level Change, vol. 58. Elsevier, pp. 1–300.
Purser, B.H., Seibold, E., 1973. The Principal Environmental Factors Influencing Holocene Sedimentation and Diagenesis. In: Purser, B.H. (Ed.), The Persian Gulf-holocene Carbonate Sedimentation and Diagenesis in a Shallow Epicontinental Sea. Springer, New York, pp. 1–9.
Reading, H.G., 1996. Sedimentary Environments: Processes, Facies and Stratigraphy, 3rd. Edition. Blackwell Science, Oxford.
Rothwell, R.G., Croudace, I.W., 2015. Twenty years of XRF core scanning marine sediments: what do geochemical proxies tell us? In: In: Croudace, I.W., Rothwell, R.G. (Eds.), Micro-XRF Studies of Sediment Cores: Applications of a Non-destructive Tool for the Environmental Sciences, vols. 25–102. Springer, Dordrecht, The Netherlands, pp. 688.
Rowlands, G., Purkis, S., 2015. Geomorphology of shallow water coral reef environments in the Red Sea. In: Rasul, N.M.A., Stewart, I.C.F. (Eds.), The Red Sea. Springer-Verlag, Berlin Heidelberg, pp. 395–408.
Roy, P.S., Thom, B.G., Wright, L.D., 1980. Holocene sequences on an embayed high-energy coast: an evolutionary model. Sediment. Geol. 26 (1–3), 1–19.
Roy, P.S., 1991. Shell hash dating and mixing models for palimpset marine sediments. Radiocarbon 33, 283–389.
Sakellariou, D., Bailey, G., Rousakis, G., Panagiotopoulos, I., Morfis, I., Georgiou, P., Momber, G., Alsharekh, A., Kalogirou, S., Stavrakakis, S., Al Nomani, S., Meredith-Williams, M., 2015. Quaternary Geology, Tectonics and Submerged Landscapes of the Farasan continental Shelf, Saudi Arabia, South Red Sea: Preliminary Results.
Sallun, A.E.M., Filho, W.S., Suguio, K., Babinski, M., Gioia, S.M.C.L., Harlow, B.A., Duleba, W., Oliveira, P.E., Garcia, V.J., Weber, C.Z., Christofoletti, S.R., Santos, C.S., Medeiros, V.B., Silva, J.B., Santiago-Hussein, M.C., Fernandes, R.S., 2012. Geochemical evidence of the 8.2 ka event and other Holocene environmental changes recorded in paleolagoon sediments southeastern Brazil. Quat. Res. 77, 31–43.
Schuhmacher, H., Kiene, W., Dullo, W.C., 1995. Factors controlling Holocene reef growth. An interdisciplinary approach. Facies 32, 145–188.
Semeniuk, V., 1995. The Holocene record of climatic, eustatic and tectonic events along the coastal zone of Western Australia - a review. J. Coast Res. 17, 247–259 Special Issue.
Siddall, M., Smeed, D.A., Matthiesen, S., Rohling, E.J., 2002. Modelling the seasonal cycle of the exchange flow in Bab el Mandab (Red Sea). Deep Sea Res. I 49, 1551–1569.
Swift, D.J., 1968. Coastal erosion and transgressive stratigraphy. J. Geol. 76 (4), 444–456.
Thom, B.G., Roy, P.S., 1985. Relative sea levels and coastal sedimentation in southeast Australia in the Holocene. J. Sediment. Res. 55 (2), 257–264.
Triantaphyllou, M.V., Pavlopoulos, K., Tsourou, Th, Dermitzakis, M.D., 2003. Brackish marsh benthic microfauna and paleoenvironmental changes during the last 6.000 years on the coastal plain of Marathon (SE Greece). Riv. Ital. Palaontol. Stratigafia 109 (3), 539–547.
Triantaphyllou, M.V., Kouli, K., Tsourou, T., Koukousioura, O., Pavlopoulos, K., Dermitzakis, M.D., 2010. Paleoenvironmental changes since 3000 BC in the coastal marsh of Vravron (Attica, SE Greece). Quat. Int. 216 (1), 14–22.
van Asselen, S., Seijmonsbergen, A.C., 2006. Expert-driven semi-automated geomorphological mapping for a mountainous area using a laser DTM. Geomorphology 78, 309–320.
Verardo, D.J., Froelich, P.N., McIntyre, A., 1990. Determination of organic carbon and nitrogen in marine sediments using the Carlo Erba NA-1500 Analyzer. Deep Sea Research Part A. Oceanogr. Res. Pap. 37 (1), 157–165.
Warren, J.K., 1991. Sulfate dominated sea-marginal and platform evaporative settings: Sabkhas and Salinas, Mudflats and Salterns. Dev. Sedimentol. 50, 69–187.
Woodroffe, C.D., Samosorn, B., Hua, Q., Hart, D.E., 2007. Incremental accretion of a sandy reef island over the past 3000 years indicated by component-specific radiocarbon dating. Geophys. Res. Lett. 34 (3).
Xiang, R., Yang, Z., Saito, Y., Fan, D., Chen, M., Guo, Z., Chen, Z., 2008. Paleoenvironmental changes during the last 8400 years in the southern Yellow Sea: benthic foraminiferal and stable isotopic evidence. Mar. Micropaleontol. 67 (1), 104–119.
Yamano, H., Abe, O., Matsumoto, E., Kayanne, H., Yonekura, N., Blanchon, P., 2003. Influence of wave energy on Holocene coral reef development: an example from Ishigaki Island, Ryukyu Islands, Japan. Sediment. Geol. 159 (1), 27–41.
Zarins, J., Murad, A.A.J., Al-Yish, K.S., 1981. The comprehensive archaeological survey program. a. The second preliminary report on the southwestern province. Atlal. J. Saudi Arab. Archaeol. 5, 9–42.